Journal of Colloid and Interface Science 368 (2012) 56–63

Contents lists available at SciVerse ScienceDirect

Journal of Colloid and Interface Science

www.elsevier.com/locate/jcis

Direct formation of iron oxide/MCM-41 nanocomposites via single or mixed *n*-alkyltrimethylammonium bromide surfactants

Kamal M.S. Khalil *, Mai M. Khalaf, Hossnia S. Mohran, Ahmed A. Elsamahy

Chemistry Department, Faculty of Science, Sohag University, 82524 Sohag, Egypt

ARTICLE INFO

Article history:
Received 10 July 2011
Accepted 11 November 2011
Available online 23 November 2011

Keywords:
Iron oxide/MCM-41
Fe_2O_3/MCM-41
Nanocomposite
TGA
DSC

ABSTRACT

Iron oxide/MCM-41 nanocomposites, Fe_2O_3/MCM-41, containing 5%, 10%, and 20% (w/w) iron oxide, were prepared via a direct nonhydrothermal method at room temperature. The preparations were preformed by using iron(III) nitrate, *tetra*-ethoxysilane (TEOS), and cetyltrimethylammonium bromide (CTAB) mixed or unmixed with dodecyltrimethylammonium bromide (DTAB). The produced materials were dried and calcined at 550 °C for 3 h. Test materials were characterized by thermogravimetric analysis (TGA), differential scanning calorimetry (DSC), Fourier transform infrared spectroscopy (FTIR), N_2 gas adsorption/desorption isotherms, small angle and wide angle X-ray diffraction (XRD). Results indicate that mixing of CTAB with DTAB does not harm the formation of blank MCM-41 structure. For the composite Fe_2O_3/MCM-41 materials, results showed formation of more stable MCM-41 structure with higher surface area and improved porosity in the presence of mixed (CTAB + DTAB) than in the presence of single (CTAB) surfactants for up to 10% Fe_2O_3/MCM-41 (w/w). This was explained in terms of the effect DTAB on contraction of the template micellar size to compensate for the expected size expansion upon the addition of ionic iron(III) nitrate precursor. Highly dispersed Fe_2O_3 nanoparticles were formed in all cases even with the highest iron oxide percentage. Formation of the nanocomposites was postulated to be determined by fast nucleation and slow growth of iron oxide species, which facilitated formation of well dispersed iron oxide nanoparticles inside and on the wall of the MCM-41 material.

1. Introduction

Since the early days of ordered mesoporous materials [1,2], there has been a growing interest in investigation of new fabrications for large number of applications. Recent investigation fields of ordered mesoporous materials include catalysis [3–10], adsorption [11], separation of nanoparticles [12], formation of nano/bio interface [13], biomedical analysis [14], drug permeation [15], electrochemical double-layer capacitor [16], rechargeable battery [17], and removal of pollutants [18]. Therefore, synthesis of ordered mesoporous materials based on the surfactant assessed approach present a very attractive area for many current researches [19]. The mesopore size of these materials is primarily controlled by the length of the alkyl chain of the surfactant used [20]. However, it was found that mixing of two alkylammonium surfactants with different alkyl chain length can be used to fine-tune the pore [21].

A wide variety of surfactants and block copolymers have been extensively studied as templates to finely tune the structure and morphology of mesoporous materials [20,22–28]. Thus, cetyltrimethylammonium bromide (CTAB) and fluorocarbon surfactant mixtures were investigated as templates [23]. Applying cationic CTAB and anionic sodium octylsulfate as templates was examined, too. It was found that the hexagonal pore size can be controlled with the mixed surfactant system [24]. Formation of mesoscopically ordered silica/mixed surfactant composites was investigated, where alkyltrimethylammonium bromide surfactants, C_nTAB, of different chain lengths as well as mixtures thereof were employed. Accordingly, a linear relationship between the mean surfactant chain length and the *d* spacing of the hexagonal phase was observed [25]. Moreover, mixed surfactant systems have also been employed in the synthesis of titanium-rich highly ordered mesoporous silica [26], synthesis of high quality mesoporous MCM-48 [27], and structurally stable MCM-48 [28]. These studies emphases the role of colloid and interface on the formation of advanced ordered materials.

The present work aims at formation of Fe_2O_3/MCM-41 nanocomposite materials via a direct, nonhydrothermal method at room temperature. Recently, several strategies have been reported [29] for the synthesis of Fe_2O_3/SiO_2 nanocomposites. The present investigation aims to explore the effect of mixing of CTAB with DTAB during the formation of the target composite materials in terms of the physical chemical aspects of colloid and interface science. Moreover, the new results are compared with the other established results reported in literature.

* Corresponding author. Fax: +20 934601159.
E-mail address: kms_khalil@yahoo.co.uk (K.M.S. Khalil).

0021-9797/$ - see front matter © 2011 Elsevier Inc. All rights reserved.
doi:10.1016/j.jcis.2011.11.027

2. Experimental

2.1. Preparation

2.1.1. Chemicals

n-Hexadecyltrimethylammonium bromide (C16TMABr), 98% Aldrich; dodecyltrimethylammonium bromide (C12TMABr), 98% Aldrich; tetraethoxysilane (TEOS), 98% $Si(OC_2H_5)_4$, Sigma–Aldrich; iron(III) nitrate, nonahydraye, $Fe(NO_3)_3.9H_2O$, Aldrich; ammonia solution, NH_4OH (33% NH_3), 99.99%, Merck; and ethyl absolute alcohol, C_2H_5OH, analytical grade product supplied by Alfa Acer, were purchased and used as received.

2.1.2. Preparation of blank MCM-41 materials with CTAB as a surfactant

Following the procedure described by Grün et al. [30], and adopted by Khalil [19]. 0.007 mol of CTAB was dissolved in 50 ml deionized water. The hydrolysis was accomplished by slowly adding 13.2 ml (0.25 mol) of aqueous ammonia, as a base catalyst, with medium stirring then 60 ml portion (1.3 mol) of absolute ethanol was added to the surfactant solution to increase homogeneity and facilitate the formation of MCM-41 spheres. The solution was stirred for 15 min at 250 *rpm* (revolution per minute) then 4.7 ml portion (0.022 mol) of TEOS was added at one time. After few minutes, turbidity started to appear and the solution turned opaque white. The solution was kept under medium stirring for 2 h; and allowed to stand for 24 h to form uniform gel. Then, the resultant gel was filtered off using Whatman filter paper and washed with 100 ml of deionized water followed by 100 ml ethanol, and left for drying overnight at 90 °C. The dried materials thus obtained were termed as *uncalcined* blank MCM-41 (abbreviated as *uncalcined* blank MCM). The material obtained by calcination of the *uncalcined* blank MCM according to the following calcination protocol: ramp at 1 °C/min from room temperature to 550 °C and hold for 3 h at 550 °C, was termed as *calcined* blank MCM-41 (abbreviated as *calcined* blank MCM).

The same calcination protocol was applied for all the calcination processes throughout this work.

2.1.3. Preparation of modified MCM-41 via mixing of CTAB with DTAB

Preparation was accomplished as above and modification was accomplished by adding of DTAB after the step of absolute ethanol addition to the surfactant solution. Modification was carried out in two ratios, namely 1:1 or 2:1 of DTAB: CTAB. After mixing, the solution was turned into opaque white gel, which was separated and treated as above to obtain the dried materials. The dried materials thus obtained were termed as uncalcined blank MCMD1 and MCMD2, where the letters "MCM" stands for MCM type of materials, the letter "D" stands for DTAB, modification, and the digit "1" or "2" stands for the DTAB: CTAB ratio as 1:1 or 2:1. Calcined materials were obtained by calcination of the uncalcined materials applying the above indicated calcinations protocol for MCM-41.

2.1.4. Preparation of Fe_2O_3/MCM-41 composite materials

Adopting a procedure analogous to the above and after dissolving of CTAB, and before ammonia addition a calculated amount of iron(III) nitrate nonahydrate was introduced as a water solution (50 ml) to satisfy 5%, 10% or 20% Fe_2O_3/MCM-41 (w/w). The preparation procedure was continued as shown above for MCM-41 and resulted in reddish brown gels in each case, which was filtered and dried. The dried materials thus obtained were termed as uncalcined 5Fe/MCM, 10Fe/MCM, and 20Fe/MCM composites. Calcined composites were obtained by calcination of the uncalcined composites as above.

2.1.5. Preparation of Fe_2O_3/MCMD composite materials

For composites preparation, only one molar mixing ratio was considered which CTAB: DTAB as 1:1, i.e., the materials MCMD1 were targeted. Thus, before the step of ammonia addition, a calculated amount of iron(III) nitrate nonahydrate was introduced as a water solution (50 ml) to satisfy 5%, 10% or 20% Fe_2O_3/MCMD1. The preparation procedure was continued as shown above for MCM-41 and resulted in reddish brown gels in each case, which was filtered and dried. The dried materials thus obtained were termed as uncalcined 5Fe/MCMD, 10Fe/MCMD, and 20Fe/MCMD composites. Calcined composites were obtained by calcination of the uncalcined composites as above.

2.2. Characterization techniques

2.2.1. Thermal analyses

A Thermal Analyst 2000 TA instrument (USA) controlling a 2050 thermogravimetric analyzer (TGA) and 2010 differential scanning calorimeter (DSC) was used. For TGA measurements, a ceramic sample boat was used with samples weighing 5.0 ± 0.1 mg. Data recorded upon heating up to 700 °C at 2 °C/min and in a stream (40 ml/min) of oxygen, or nitrogen gas as indicated. For DSC measurements, a sample size of 5.0 ± 0.1 mg was heated up to 550 °C in a covered aluminum sample pan at 10 °C/min and a flow of 40 ml/min of oxygen, or nitrogen gas.

2.2.2. FTIR spectroscopy

FTIR spectra for the test materials were carried out using KBr disk technique using an FTIR spectrometer, model Shimadzu-FTIR800 (Japan), in the range 4000–400 cm^{-1}, with 40 scans and a resolution of 4 cm^{-1}.

2.2.3. X-ray diffraction (XRD)

XRD patterns were obtained using a Philips 1840 diffractometer at room temperature using Cu Kα radiation. Diffraction patterns were obtained with Ni-filtered Cu Kα radiation (λ = 0.15418 nm).

2.2.4. Electron microscopy

TEM micrographs were carried out, using a model JEM-1010 Joel microscope operated at 80 kV, to investigate the calcination products. Test samples were prepared by ultrasonic dispersion of the solid in alcohol. A drop of the resulting suspension was doped to a carbon coated grids.

2.2.5. Nitrogen gas adsorption/desorption

Surface area and pore size information was obtained from nitrogen adsorption/desorption isotherms at 77 K, using a Micromeritics ASAP 2000 (Accelerated Surface Area and Porosimetry analyzer, USA). Prior to measurement, all samples were degassed to 0.1 Pa and 150 °C for 2 h. Porosity distribution in the mesopore range was generated by the BJH analysis [31] using the instrument software. Assessments of microporosity were made from *t*-plot constructions, using the Harkins–Jura correlation [32] for *t*-thickness as a function of normalized pressure, p/p_o. *t*-plot surface areas, S_t, were calculated from slope analysis of the *t*-plots according to the standard methods [33]. The micropore surface area, S_{mic}, area corresponding to the gas condensed in micropores, was calculated as $S_{mic} = S_{BET} - S_t$.

3. Results and discussion

3.1. Characterization of the uncalcined materials

Thermogravimetric analysis was carried out for the uncalcined materials. TGA and DTG curves for the uncalcined blank MCM

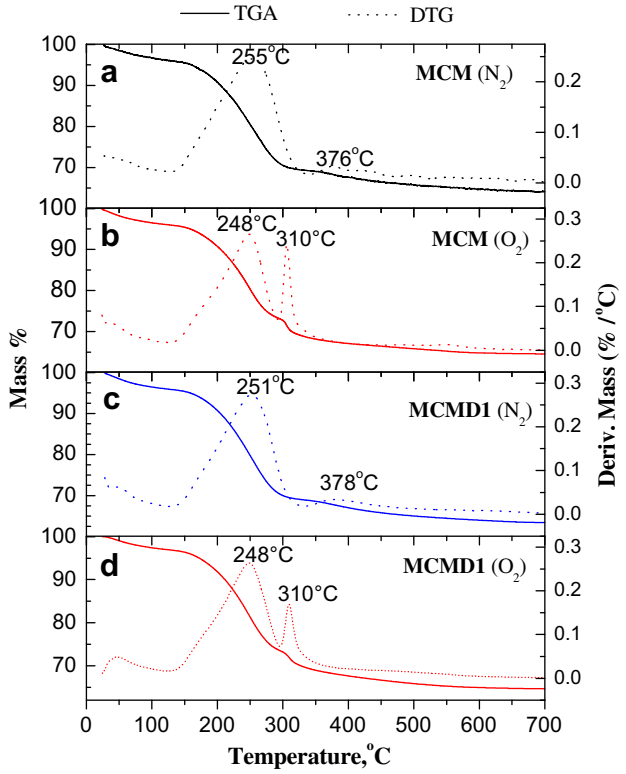

Fig. 1. TGA and DTG curves for the uncalcined blank MCM material (a) in flow of N_2 gas, (b) in flow of O_2; as well as for the uncalcined blank MCMD1 material (c) in flow of N_2 gas, and (d) in flow of O_2.

and MCMD1 in flow of N_2 (or O_2) atmosphere are shown in Fig. 1. Total mass loss recorded upon heating over the temperature range of RT-700 °C was 36.2% in N_2 flow (31.0% in flow of O_2) for MCM. DTG curve suggests that mass loss process and evolution of the MCM-41 structure occurred through a four steps process. Each step limits and mass loss were very sensitive for the type of atmosphere (N_2 or O_2 gas) as shown in Table 1. Further thermal analyses, data are given in Table S1. Based on the thermal analysis studies reported for similar systems [19,34], the first step below 120 °C is assignable for the loss of the adsorbed and included water molecules and/or organic solvents. This was followed by two steps maximize at 255 °C and 376 °C in flow of N_2 gas (at 248 °C, 310 °C in flow of O_2 gas), which represent the major portion of mass loss process (29.5% out of 36.2% in flow of N_2; and 26.1% out of 31.0% in flow of O_2) and they are mainly assignable for the removal of the template surfactant. See below, FTIR results Fig. 5 for the uncalcined and calcined materials, which indicated that upon calcinations over the range of 120–400 °C, the materials loss organic groups of the surfactants. Finally, the fourth step of the mass loss process amounting to 2.0% in flow of N_2 (1.3% in flow of O_2) may be assign for the removal of heavy carbon containing species. These results are in agreement with the reported mechanism for template removal that based on Hofmann degradation below 260 °C, which followed by decomposition and/or combustion reaction above 260 °C [34]. Therefore, the peak observed at 376 °C in N_2 gas flow, which shifted to 310 °C and sharpened in O_2 gas flow, is indicative that the nature of process was changed from decomposition (in N_2) to combustion (in O_2).

TGA and DTG curves for the uncalcined MCMD1 in flow of N_2 and in flow of O_2 atmosphere are shown in Fig. 1. Total mass loss, over the temperature range of RT-700 °C was 36.6% in N_2 flow (35.7% in flow of O_2) for MCMD1. The sequence of the thermal events can be explained as for the above blank MCM case in terms of the four steps

Table 1
TGA Results for uncalcined blank and composite materials obtained in flow of N_2 and O_2 gas.

Materials	Nitrogen flow		Oxygen flow	
	ΔW (%)	T_{max} (°C)	ΔW (%)	T_{max} (°C)
MCM	36.2	255, 376	31.0	248, 310
MCMD1	36.6	251, 378	35.7	248, 310
MCMD2	37.2	250, 387	37.4	248, 312
5Fe/MCM	29.6	259, 463	30.5	252, 313, 427
10Fe/MCM	23.7	278, 450, 560	23.3	276, 314, 419
20Fe/MCM	22.6	278, 354, 526	23.2	274, 310
5Fe/MCMD	31.2	271, 451	31.9	267, 315, 421
10Fe/MCMD	27.7	277, 456	26.7	280, 322, 436
20Fe/MCMD	27.0	272, 345, 492	25.8	276, 320

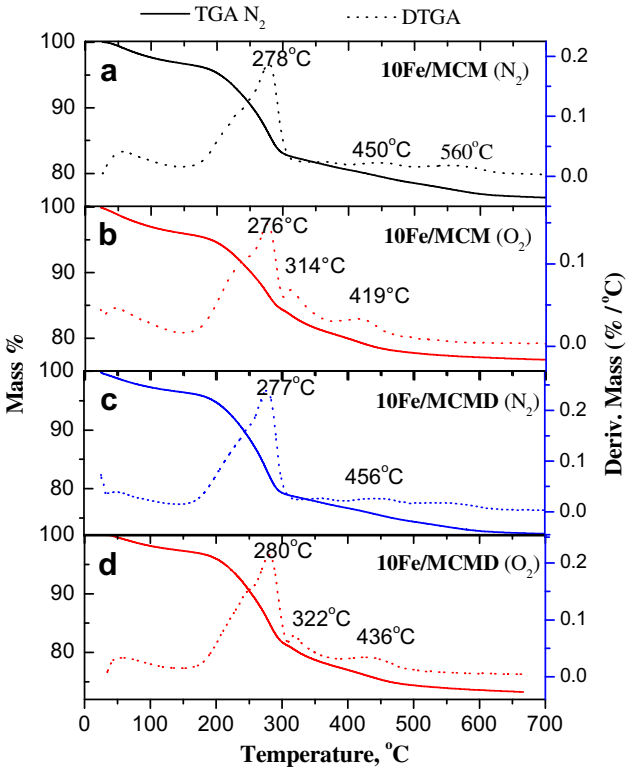

Fig. 2. TGA and DTG curves for the uncalcined 10Fe/MCM material (a) in flow of N_2 gas, (b) in flow of O_2; as well as for the uncalcined 10Fe/MCMD material (c) in flow of N_2 gas, and (d) in flow of O_2.

process, see Table S1. It is important to notice that the mass loss in flow of O_2 gas is closer to that in N_2 gas flow for MCMD1 than for MCM. This suggests that mixing of the two surfactants improves combustion and removal of the template. Results for MCMD1 and MCMD2 can be observed in Table 1, further data are given in Table S1. It is noticeable that mass losses recorded for the blank materials were in the order of MCMD2 > MCMD1 > MCM. This indicates that more template molecules were included in silica matrix upon mixing of the CTAB with DTAB in 1:2 or 1:1 molar ratio, respectively.

TGA and DTG curves for the uncalcined composite material (10Fe/MCM and 10Fe/MCMD) in flow of N_2 and O_2 are shown in Fig. 2, as representatives. Mass loss for 10Fe/MCM over the temperature range of RT- 700 °C was 23.7% in flow of N_2 (23.3% in flow of O_2) gas. The main mass loss steps for the removal of the template were characterize by peaks at 278, 450 and 560 °C for 10Fe/MCM in flow of N_2 (shifted to 276, 314 and at 419 °C in flow of O_2) gas.

For the composite materials prepared with mixed surfactants, total mass loss over the range RT-700 °C for 10Fe/MCMD was 27.7% in flow of N_2 (26.7% in flow of O_2) gas, Fig. 2. The main mass

loss steps for the removal of the template were characterize by two peaks at 277 and 456 °C in flow of N_2 gas (three peaks at 280, 322, and 436 °C in flow of O_2) gas. Detailed results for the 5, 10, 20Fe/MCM and 5, 10, 20Fe/MCMD are cited in Table 1, whereas further data are given in Table S1. It is interesting for the two composite groups obtained with single or mixed surfactants that mass loss decreases with the increasing of iron oxide contents, either in N_2 or O_2 flow. This means that less template molecules were included with the increasing of iron oxide contents. Moreover, mass loss in N_2 flow is greater than in O_2 flow for the second group of composite materials (10Fe/MCMD and 20Fe/MCMD but not for 5Fe/MCMD). This is probably due to partial reduction of iron oxide species in N_2 flow conditions and full oxidation of iron species in flow of O_2 gas. This was because in N_2 atmosphere (absence of O_2) the decomposition/composition processes of the precursor materials may produce incomplete oxidation products such as CO gas and carbonous materials.

DSC analysis was carried out for the uncalcined materials. Results for the uncalcined blank MCM, MCMD1 along with the 10Fe/MCM composite in flow of N_2 gas are shown in Fig. 3 (top). For the uncalcined MCM, an endothermic peak was observed at ~ 230 °C which followed by an exothermic one at ~420 °C. Similar behaviors were observed for the uncalcined MCMD1. These two peaks are in good agreement with the TGA peaks observed in flow of N_2 atmosphere at 255 °C and 376 °C (Fig. 1), which assigned for the two steps removal of surfactant. For 10Fe/MCM composite in flow of N_2, Fig. 3 (top), an endothermic peak close to 230 °C along with two exothermic peaks close to 310 and 400 °C where observed. This indicates that iron precursor affected the template removal process even in flow of N_2 gas.

When DSC measurements were carried out in flow of O_2 atmosphere, no much difference was observed for the blank samples. However, uncalcined 10Fe/MCM, Fig. 3 (bottom), showed two exothermic peaks at 290 °C and 400 °C (instead of at 310 and 400 in flow of N_2 gas flow). Such shift confirms the combustion nature of the first peak. Furthermore, for 20Fe/MCM, Fig. 3 (bottom), a convoluted large broad peak maximize at 312 °C was observed, probably due to the large amount of iron precursor species in the uncalcined composite materials (see FTIR results below). This pronounced effect of iron precursor on the behaviors of the DSC thermograph indicates that iron species are very reactive and suggests that they are finely divided and well dispersed (see XRD results below). DSC of the uncalcined 10Fe/MCMD and 20Fe/MCMD in flow of N_2 and O_2 are shown in Fig. 4. DSC results of the uncalcined Fe/MCMD materials are similar to the above case of uncalcined Fe/MCM materials, thus similar conclusion can be made.

FTIR spectra for the uncalcined blank and composite materials were carried out. Some representative spectra are shown in Fig. 5. The spectrum for the uncalcined blank materials (spectrums a and b, respectively), exhibit a group of strong intense bands at 3475, 2929, 1636, and 1475 cm^{-1} as well as a group of bands in the region below 1400 cm^{-1}. The bands at 3475 and 1630 cm^{-1} are assignable for the stretching mode and bending mode of adsorbed water molecules, the band at ~2929 cm^{-1} is assignable for the stretching mode of $\upsilon CH(-CH_3)$ and $\upsilon CH(-CH_2-)$ groups of the template species respectively [35,36]. The band at 1475 cm^{-1} is assignable for the bending mode of $\delta CH(-CH_3)$ and $\delta CH(-CH_2-)$ groups. The group of bands observed below 1400 cm^{-1} is assignable for the frame work vibration of Si-MCM-41 [35,36]. FTIR spectra for some uncalcined composite materials are shown in Fig. 5 (spectrums c–e). Where, an additional band at 1399 cm^{-1} was developed, specially, for the latter two spectrums, which represent high amounts of the iron precursor. Therefore, this band may be attributed to adsorbed ammonia and/or nitrate species.

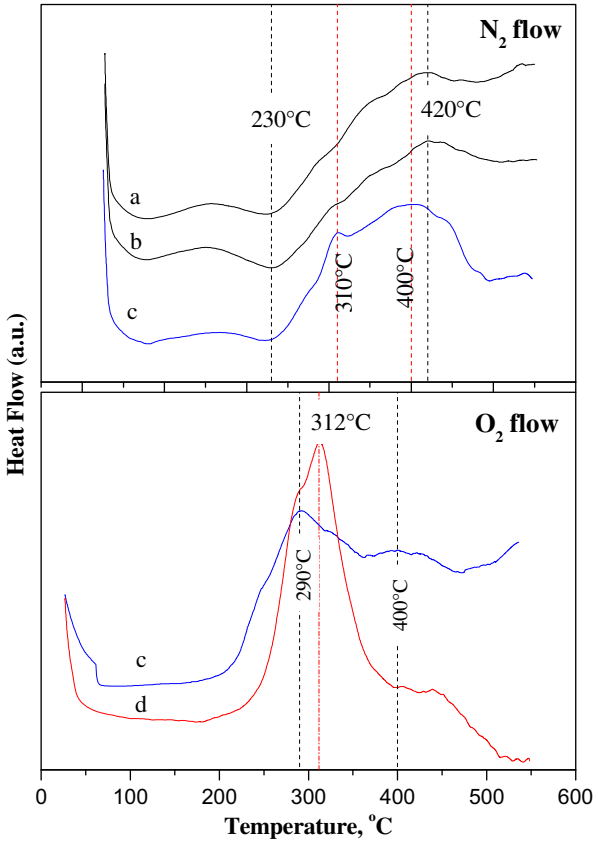

Fig. 3. DSC curves for the uncalcined (a) MCM, (b) MCMD and 10Fe/MCM in flow of N_2 gas (top); (c) 10Fe/MCM and (d) 20Fe/MCM materials in flow of O_2 gas (bottom).

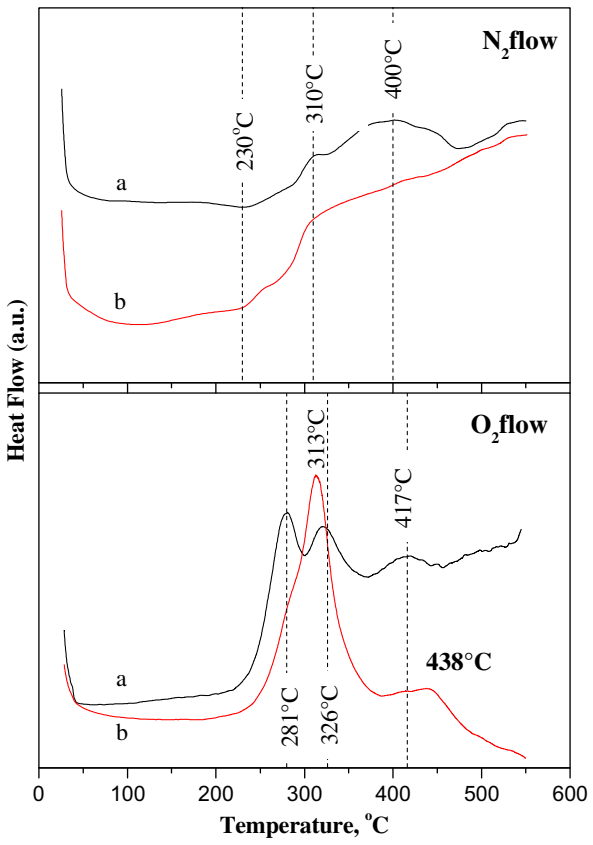

Fig. 4. DSC curves for the uncalcined (a) 10Fe/MCMD and (b) 20Fe/MCMD materials in flow of N_2 gas (top) or in flow of O_2 gas (bottom).

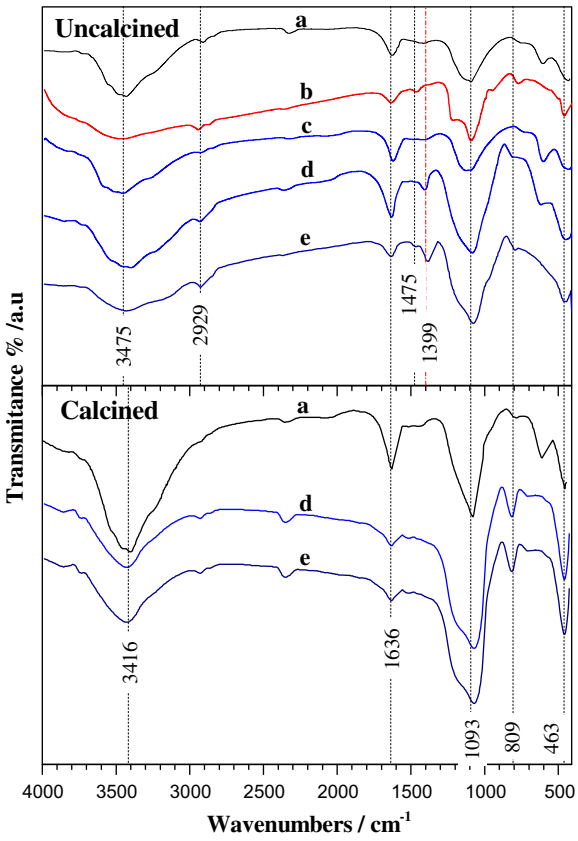

Fig. 5. FTIR Spectra for uncalcined (top) and calcined (bottom) materials: (a) blank MCM, (b) MCM1, (c) 5Fe/MCM, (d) 20Fe/MCM, and (e) 20Fe/MCMD.

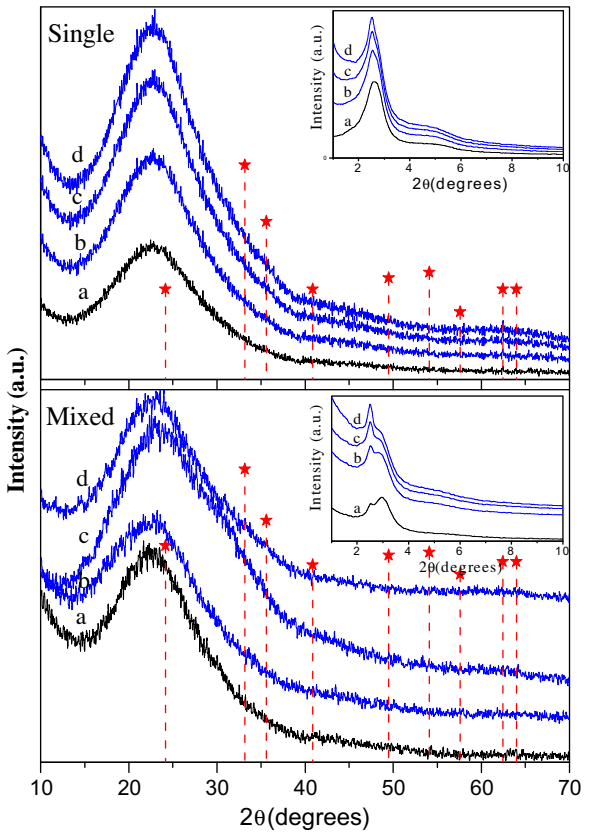

Fig. 6. (Top plate) Wide angle XRD, WAXRD for the calcined materials obtained with a single surfactant: namely (a) blank MCM, (b) 5Fe/MCM, (c) 10Fe/MCM, and (d) 20Fe/MCM; the insert shows small angle XRD, SAXRD for the same set of materials. (Bottom plate) WAXRD for the calcined materials obtained with a mixed surfactants: namely (a) blank MCMD1, (b) 5Fe/MCMD, and (c) 10Fe/MCMD, (d) 20Fe/MCMD; the insert shows SAXRD for the same set of materials. The stars position with drop lines represent the standard diffraction data for hematite Fe_2O_3, file no. 33-0664.

3.2. Bulk characterization of the calcined materials

FTIR spectra for the calcined material were carried out. Some representative spectra are shown in Fig. 5 (bottom). The spectra indicate that the bands related to the template species have been removed, and the remaining vibration bands are characteristic for MCM-41 type of materials. Thus, the band at 1093 cm^{-1} is assigned to υ_{as}(-Si—O—Si), the weak band at 809 cm^{-1} is assigned to υ_s(Si—O—Si), and the band at 463 cm^{-1} is assigned to δ(Si—O—Si). [36–38]. It is notable that a weak band was observed at 680 cm^{-1} for 20Fe/MCM, and 20Fe/MCMD. However, Si—O—Fe species are characterized by two bands at 660 cm^{-1} and 960 cm^{-1} [39,40].

Wide angle XRD, WAXRD patterns for the calcined materials obtained with a single surfactant are shown in Fig. 6 (top plate). Small angle XRD, SAXRD patterns of the same set of materials are inserted. WAXRD for the calcined materials obtained with mixed surfactants are shown in Fig. 6 (bottom plate). SAXRD for the same set of materials are inserted. The stars position with drop lines shown in Fig. 6, represent the standard diffraction data for hematite Fe_2O_3, file no. 33-0664 [41].

SAXRD patterns show a main peak corresponding to diameter of 33.6 Å, 30.3 Å or 29.6 Å, respectively for blank MCM, MCMD1, and MCMD2 materials. This indicates that preparations carried out with mixed surfactants resulted in smaller pore size and this effect increase with increase of DTAB ratio. This significant modification is in agreement with the basic concepts of colloids and surface science which implies a smaller micellar size upon mixing of a surfactant with similar one having a smaller tail.

For the calcined 5Fe/MCM and 20Fe/MCM materials, the main peaks corresponds to 35.6 Å and 36.0 Å, respectively. For the calcined 5Fe/MCMD and 20Fe/MCMD, the peak corresponds to 35.4 or 36.0 Å, respectively. This slight increase in pore diameter with the increase of iron oxide precursor indicates that the later may play a role in larger micelle formation thereby led to widening of porosity.

WAXRD patterns for the calcined blank and composites materials are shown in Fig. 6. While Fe_2O_3 is a certain product under the applied basic conditions, no sharp peaks characteristic for crystalline Fe_2O_3 were observed. Nevertheless, there are some broadening at the main peaks positions for hematite iron oxide (file no. 33-0664) [41]. These lines broadening are best shown against the blank materials. This situation might arises because, iron oxide present as finely dispersed nano dimensional particles (at least in one dimension) below the detection limits of x-ray and/or as amorphous particles that give no diffraction peaks. In fact, this reflects the success of the method in dispersing iron oxide phase in the MCM-41 silica matrix and stabilizing it up to the applied calcination temperature.

It should be noted that formation of Fe_2O_3/MCM-41 composite is much more favor than the formation of Fe-MCM-41. This was because the preparation was carried out in basic conditions. Monomeric octahedral aquo-hydroxocomplexes which is the precursor for ion exchange of iron are stable only at pH < 2 [42]. Moreover, It has been reported recently that the color of the Fe-MCM-41 materials is all white [43], while our samples were reddish brown. This confirms that Fe_2O_3/MCM-41 should be formed under the present basic condition not Fe-MCM-41.

3.3. Surface characterization of the calcined materials

Nitrogen adsorption/desorption isotherms for blank materials MCM, MCMD1, and MCMD2 are shown in Fig. 7. The isotherms

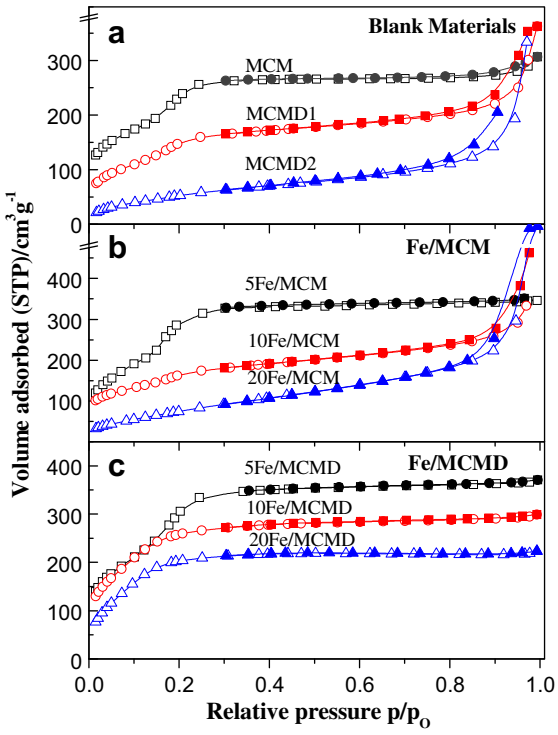

Fig. 7. Nitrogen adsorption/desorption isotherms for the calcined (a) blank materials: MCM, MCMD1, and MCM2; (b) Fe/MCM materials: 5Fe/MCM, 10Fe/MCM, 20Fe/MCM; and (c) Fe/MCMD materials 5Fe/MCMD, 10Fe/MCMD, and 20Fe/MCMD.

can be classified as type **IV** of isotherms, which is characteristic for MCM-41 materials [44]. Specific surface area amounts to 1167 $m^2 g^{-1}$, 1024 and 997 $m^2 g^{-1}$, were calculated for the three blank materials, respectively. Further structural data are cited in Table 2. Results indicate that mixing of CTAB with DTAB does not harm the MCM-41 structure. However, little decrease in S_{BET} value was observed which may be attributed to the formation of smaller micellar size and thereby smaller pore size due to the presence of two surfactants [45]. This explanation is in agreement with the total pore volume, V_p values, obtained for the above materials as cited in Table 2.

Nitrogen adsorption isotherms for the composite materials formed in the presence of CTAB as a single surfactant (calcined 5Fe/MCM, 10Fe/MCM, and 20Fe/MCM) are shown in Fig. 7. The isotherms are classified as type **IV** of isotherms characteristics for MCM-41, specially, for the first composite. S_{BET} amounting to 652, 500 and 304 $m^2 g^{-1}$, were calculated for the indicated composite materials, respectively. Thus, on comparison with the corresponding blank MCM material, one can recognize decreasing of S_{BET} values while increasing of V_p and W_p values. Increasing of the latter two parameters may be attributed to the role of iron salt precursor in increasing of micelles size due to the presence of the charged ions of iron salt [45]. Whereas, decreasing of S_{BET} with increasing of the loading ratio of Fe_2O_3 in the MCM-41 may be explained in terms of pore blocking of MCM-41 matrix due to the presence of Fe_2O_3 particles and their aggregates. Moreover, loading of much more iron oxide precursor inside the pores, led to collapse of the MCM-41 structure, probably, during heat treatment (due to evolution of increasing amount of evolved gas). In the present work, it seems that 10% loading is the optimum value, i.e., high loading percentage while preserving MCM-41 structure. For 20% loading, collapse of the ordered porous structure was occurred. This conclusion was supported by N_2 adsorption isotherms which characterize the formation of open surfaces (i.e., distraction of MCM-41) rather than ordered mesoporous structure for 20% loading materials.

Nitrogen adsorption isotherms for the composite materials formed in the presence of CTAB mixed with DTAB (5Fe/MCMD, 10Fe/MCMD, and 20Fe/MCMD) are shown in Fig. 7. Isotherms type characteristics for MCM-41 material were obtained. S_{BET}, amount to 719, 582, and 269 $m^2 g^{-1}$, respectively were calculated for the three composite materials, respectively. Further structural data are cited in Table 2. However, these values are better than that observed for 5Fe/MCM and 10Fe/MCM. This indicates that modification with DTAB was helpful for satisfactory preservation of MCM-41 structure for up to 10% loading of Fe_2O_3. This may be attributed to opposing of the micellar size increasing (due to presence of NO_3^- ions and destruction of MCM-41 structure) by decreasing of micellar size due to the mixing effect of the surfactants.

As a test for microporosity, *t*-plot analysis was performed on the adsorption branches of the isotherms obtained with the test calcined materials. The plots results are cited in Table 2. Accordingly, S_{mic} amounting to $\leqslant 23$ $m^2 g^{-1}$ against S_t amounting to $\geqslant 974$ $m^2 g^{-1}$ were obtained with the blank materials (MCM, MCMD1, and MCMD2) thus indicating predominance of mesoporosity.

The composite materials formed in the presence of CTAB as a single surfactant (5Fe/MCM, 10Fe/MCM, and 20Fe/MCM) showed

Table 2
Textural characteristics for calcined blank and composite materials, along with some recently published results for similar materials obtained with different methods.

Materials	S_{BET} ($m^2 g^{-1}$)	V_p ($cm^3 g^{-1}$)	*t*-Method ($m^2 g^{-1}$)		Pore width, W_p (Å)	
			S_{mic}	S_t	4 V/S_{BET}	BJH
MCM	1167	0.567	15	1152	19.5	21.3
MCMD1	1024	0.457	16	1008	17.8	17.7
MCMD2	997	0.416	23	974	16.7	18.2
5Fe/MCM	652	0.515	8	644	21.0	23.8
10Fe/MCM	500	0.518	140	360	52.2	72.5
20Fe/MCM	304	0.515	74	230	163.5	173
5Fe/MCMD	719	0.427	14	705	23.7	24.3
10Fe/MCMD	582	0.425	107	475	38.5	47.2
20Fe/MCMD	269	0.426	135	134	108.5	134
3% Fe_2O_3/MCM-41 540 °C/5 h (H, D) [43]	981	0.925	596	385	13.7	
~5% Fe_2O_3/MCM-41 550 °C/1 h (H, P) [44]	376	0.21	NA	NA	35.6	
5% Fe_2O_3/MCM-41(R) 325 °C/1 h (H, D) [45]	775	24.8	NA	NA	16.7	
Fe_2O_3/SBA-15/1 450 °C/10 h (incip. wet., nit) [46]	770	NA	53	717		

The preparation method is indicated between brackets (): H = hydrothermal, D = direct, P = post synthesis. NA indicates "not available" data.

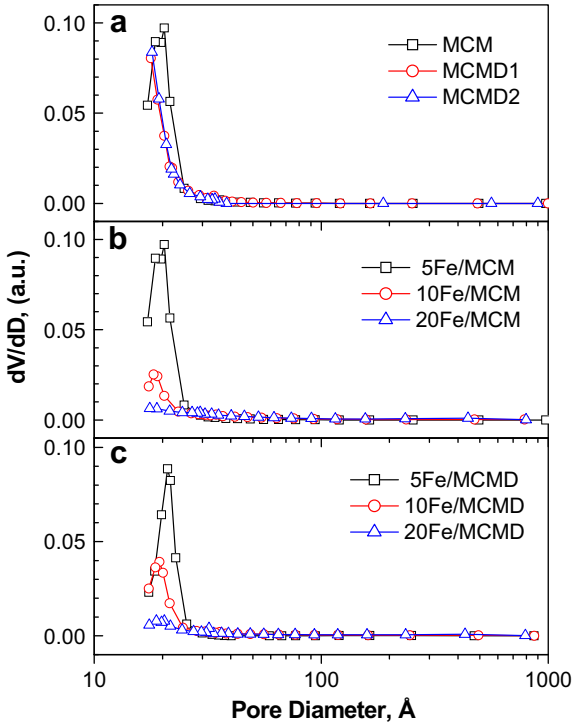

Fig. 8. BJH pore width distribution derived from N_2 Nitrogen adsorption/desorption isotherms for the calcined (a) blank materials: MCM, MCMD1, and MCM2; (b) Fe/MCM materials: 5Fe/MCM, 10Fe/MCM, 20Fe/MCM; and (c) Fe/MCMD materials 5Fe/MCMD, 10Fe/MCMD, and 20Fe/MCMD.

S_{mic} values amounting to 8, 140, and 74 $m^2\ g^{-1}$ against S_t amounting to 644, 360, and 230 $m^2\ g^{-1}$, respectively. However, the composite materials formed in the presence of CTAB and DTAB as mixed surfactants (5Fe/MCMD, 10Fe/MCMD, and 20Fe/MCMD) showed S_{mic} amounting to 14, 107, and 135 $m^2\ g^{-1}$ against to S_t amounting to 705, 475, and 134 $m^2\ g^{-1}$, respectively. Thus, predominance of mesoporosity can tentatively be postulated for composites 5Fe/MCM from the single surfactant group, as well as for 5Fe/MCMD and 10Fe/MCMD from the mixed surfactant group.

Pore width, W_p via the average ($4V_p/S_{BET}$) and BJH methods were obtained and peak maximum were cited in Table.2. Pore width distribution for the calcined blank and composite materials obtained with CTAB or CTAB + DTAB are shown in Fig. 8.

A mono PWD maximize at 21.3 Å was obtained for the calcined blank MCM material. The PWD was shifted toward micropore region for MCMD1 and MCMD2 blank materials as expected due to the proposed decrease of micelle size.

Mono PWD were also observed for the calcined composite materials obtained with single or mixed surfactants, where the pore width was increased with increasing of iron oxide ratio. Thus indicating that loading of iron oxide in the frame of MCM-41 led to widening of mesoporosity. The broad and low intensity PWD peaks which were observed for high iron oxide content composites may be due to the collapse of some walls and formation of channels with larger pore width.

At the end, to evaluate the performance of the present method, the data obtained for the test group of materials were compared with data reported in some recent literatures for similar Fe_2O_3/MCM-41 composites obtained by other methods [46–49]. These data are cited in Table 2. It is clear that the present direct method yielded products of higher S_{BET}, preserves MCM-41 structure, preserves mesoporosity and prevents microporosity.

Finally, TEM micrograph for the blank MCM and MCMD1 were typical and showed a matrix of aggregated and agglomerated spherical particles with nearly equal size (not shown). Fig. 9 shows the morphology of the 10Fe/MCM sample as a case of some spherical MCM particles and partial distortion of others. The fine structure of this sample appears as a matrix composed of spherical and irregular silica particulates embedded with very many small irregular dark dots represent Fe_2O_3 nanoparticles and their aggregates. Similar observation of a highly anisotropic distribution of iron nanoparticles within MCM-41 mesoporous silica has been observed via direct observation by electron microscopy techniques [50].

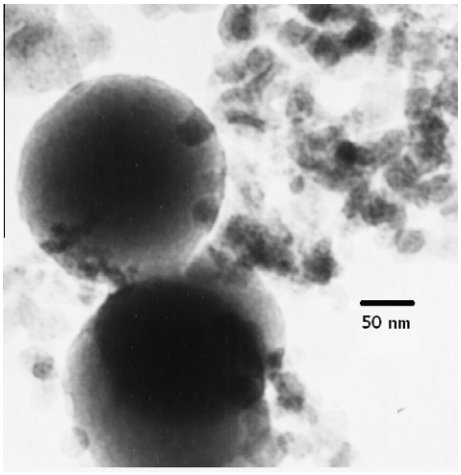

Fig. 9. TEM micrograph for the calcined: 10Fe/MCM.

4. Conclusions

Ordered mesoporous materials were successfully formed via surfactant template method with single (CTAB) or mixed (CTAB + DTAB) surfactants. It was found that mixing of the two surfactants improves combustion and removal of the template.

Stable Fe_2O_3/MCM-41 composites (for at least 10% w/w) with well dispersed isolated and/or aggregated nanoparticles of Fe_2O_3 within the MCM-41 structure were formed. It was found that higher S_{BET} value was observed for composites obtained with mixed surfactants than composites obtained with a single surfactant. Moreover, mixing of the two surfactants tunes and improves porosity of the Fe_2O_3/MCM-41 composites. This confirms the presence of a linear relationship between the mean surfactant chain length and the pore width [25].

The present method, which is direct and carried out at room temperature, produces materials with better surface parameters than those obtained by other hydrothermal methods [46–49]. Moreover, the titled composite materials can be prepared in small or large amounts and used as is or applied to other supports. This opens large opportunity for its benefits for various surface science applications.

Appendix A. Supplementary material

Supplementary data associated with this article can be found, in the online version, at doi:10.1016/j.jcis.2011.11.027.

References

[1] C.T. Kresge, M.E. Leonowicz, W.J. Roth, J.C. Vartuli, J.S. Beck, Nature 359 (1992) 710.
[2] J.S. Beck, J.C. Vartuli, W.J. Roth, M.E. Leonowicz, C.T. Kresge, K.D. Schmidt, C.T.-W. Chu, D.H. Olson, E.W. Sheppard, S.B. McCullen, J.B. Higgins, J.C. Schlenker, J. Am. Chem. Soc. 114 (1992) 10834.

[3] S.B. Bukallah, A. Bumajdad, K.M.S. Khalil, M.I. Zaki, Appl. Surf. Sci. 256 (2010) 6179.
[4] F. Shang, H. Liu, J. Sun, B. Liu, C. Wang, J. Guan, Q. Kan, Catal. Commun. 12 (2011) 739.
[5] Y. Ding, H. Sun, J. Duan, P. Chen, H. Lou, X. Zheng, Catal. Commun. 12 (2011) 606.
[6] S. Sisodiya, S. Shylesh, A.P. Singh, Catal. Commun. 12 (2011) 629.
[7] D. Meloni, R. Monaci, Z. Zedde, M.G. Cutrufello, S. Fiorilli, I. Ferino, Appl. Catal. B: Environ. 102 (2011) 505.
[8] M. Kollár, I. Kolev, M.R. Mihályi, V. Mavrodinova, Appl. Catal. A: Gen. 393 (2011) 59.
[9] X. Yang, S. Liao, J. Zeng, Z. Liang, Appl. Surf. Sci. 257 (2011) 4472.
[10] Y. Xia, H. Dai, H. Jiang, L. Zhang, J. Deng, Y. Liu, J. Hazard. Mater. 186 (2011) 84.
[11] Y. Zhao, Q. Gao, T. Tang, Y. Xu, D. Wu, Mater. Lett. 65 (2011) 1045.
[12] M.M. Mekawy, A. Yamaguchi, S.A. El-Safty, T. Itoh, N. Teramae, J. Colloid Interface Sci. 355 (2011) 348.
[13] H.K. Baca, E.C. Carnes, C.E. Ashley, D.M. Lopez, C. Douthit, S. Karlin, C.J. Brinker, Biochim. Biophys. Acta 1810 (2011) 259.
[14] H. Kataoka, K. Saito, J. Pharm. Biomed. 54 (2011) 926.
[15] L.M. Bimbo, E. Mäkilä, T. Laaksonen, V.-P. Lehto, J. Salonen, J. Hirvonen, H.A. Santos, Biomaterials 32 (2011) 2625.
[16] Q. Li, R. Jiang, Y. Dou, Z. Wu, T. Huang, D. Feng, J. Yang, A. Yu, D. Zhao, Carbon 49 (2011) 1248.
[17] X. Liang, Z. Wen, Y. Liu, H. Zhang, L. Huang, J. Jin, J. Power Sources 196 (2011) 3655.
[18] X. Fu, X. Chen, J. Wang, J. Liu, Microporous Mesoporous Mater. 139 (2011) 8.
[19] K.M.S. Khalil, J. Colloid Interface Sci. 315 (2007) 562.
[20] A. Taguchi, F. Schuth, Microporous Mesoporous Mater. 77 (2005) 1.
[21] S. Namba, A. Mochizuki, M. Kito, Chem. Lett. (1998) 569.
[22] D.Y. Zhao, J.L. Feng, Q.S. Huo, N. Melosh, G.H. Fredrickson, B.F. Chmelka, G.D. Stucky, Science 279 (1998) 548.
[23] C.X. Lin, P. Yuan, C.Z. Yu, S.Z. Qiao, G.Q.M. Lu, Microporous Mesoporous Mater. 126 (2009) 253.
[24] T. Ohkubo, T. Ogura, H. Sakai, M. Abe, J. Colloid Interface Sci. 312 (2007) 42.
[25] I. Beurroies, P. Agren, G. Büchel, J.B. Rosenholm, H. Amenitsch, R. Denoyel, M. Linden, J. Phys. Chem. B 110 (2006) 16254.
[26] D. Chandra, N. Kishor Mal, M. Mukherjee, A. Bhaumik, J. Solid State Chem. 179 (2006) 1802.
[27] F.-Y. Wei, Z.-W. Liu, J. Lu, Z.-T. Liu, Microporous Mesoporous Mater. 131 (2010) 224.
[28] C. Liu, S. Wang, Z. Rong, X. Wang, G. Gu, W. Sun, J. Non-Cryst. Solids 356 (2010) 1246.
[29] K.M.S. Khalil, H.A. Mahmoud, T.T. Ali, Langmuir 24 (2008) 1037.
[30] M. Grün, K.K. Unger, A. Matsumoto, K. Tsutsumi, Microporous Mesoporous Mater. 27 (1999) 207.
[31] E.P. Barrett, L.G. Joyner, P.P. Halenda, J. Am. Chem. Soc. 73 (1951) 373.
[32] W.D. Harkins, G. Jura, J. Am. Chem. Soc. 66 (1944) 01366.
[33] B.C. Lippens, J.H. de Boer, J. Catal. 4 (1965) 319.
[34] F. Kleitz, W. Schmidt, F. Schüth, Microporous Mesoporous Mater. 65 (2003) 1.
[35] I.A. Degen, Tables of Characteristic Group Frequencies for the Interpretation of Infrared and Raman Spectra, Acolyte Publication, Harrow, UK, 1997.
[36] Y. Zheng, Z. Li, Y. Zheng, X. Shen, L. Lin, Mater. Lett. 60 (2006) 3221.
[37] S.C. Laha, P. Mukherjee, S.R. Sainkar, R. Kumar, J. Catal. 207 (2002) 213.
[38] W. Yao, Y. Chen, L. Min, H. Fang, Z. Yan, H. Wang, J. Wang, J. Mol. Catal. A: Chem. 246 (2006) 162.
[39] J.S. Choi, S.S. Yoon, S.H. Jang, W.S. Ahn, H.J. Choi, Stud. Surf. Sci. Catal. 158 (2005) 1405.
[40] Z.Y. Yuan, S.Q. Liu, T.H. Chen, J.Z. Wang, H.X. Li, J. Chem. Soc. Chem. Commun. (1995) 973.
[41] JCPDS, International Centre for Diffraction Data, PCPDFWIN, JCPDS-ICDD, 1995.
[42] G. Perego, R. Millini, G. Bellussi, Synthese (1998) 187.
[43] B. Li, J. Xu, J. Liu, S. Zuo, Z. Pan, Z. Wu, J. Colloid Interface Sci. 366 (2012) 114.
[44] F. Rouquerol, J. Rouquerol, K. Sing, Adsorption by Powders and Porous Solids, Academic Press, London, 1999. p. 415.
[45] D.J. Shaw, Introduction to Colloids and Surface Science, fourth ed., Butterworth-Heienemann, Oxford, 1998. p. 84–90.
[46] Z.Y. Yuan, W. Zhou, Z.L. Zhang, Q. Chen, B.-L. Su, L.-M. Peng, Stud. Surf. Sci. Catal. 141 (2002) 403.
[47] A. Bhaumik, S. Samanta, N.K. Mal, PRAMANA-J. Phys. 65 (2005) 855.
[48] J.F. Bengoa, M.V. Cagnoli, N.G. Gallegos, A.M. Alvarez, L.V. Mogni, M.S. Moreno, S.G. Marchetti, Microporous Mesoporous Mater. 84 (2005) 153.
[49] S. Valange, R. Palacio, A. Charmot, J. Barrault, A. Louati, Z. Gabelica, J. Mol. Catal. A: Chem. 305 (2009) 24.
[50] M.S. Morenoa, M. Weyland, P.A. Midgley, J.F. Bengoa, M.V. Cagnoli, N.G. Gallegosc, A.M. Alvarez, S.G. Marchetti, Micron 37 (2006) 52.